

<https://doi.org/10.1038/s42005-024-01618-5>

Superconducting diode effect sign change in epitaxial Al-InAs Josephson junctions

Check for updates

Neda Lotfizadeh¹, William F. Schiela¹, Barış Pekerten^{2,3}, Peng Yu¹, Bassel Heiba Elfeky¹, William M. Strickland¹, Alex Matos-Abiague² & Javad Shabani¹ ✉

There has recently been a surge of interest in studying the superconducting diode effect (SDE) partly due to the possibility of uncovering the intrinsic properties of a material system. A change of sign of the SDE at finite magnetic field has previously been attributed to different mechanisms. Here, we observe the SDE in epitaxial Al-InAs Josephson junctions with strong Rashba spin-orbit coupling (SOC). We show that this effect strongly depends on the orientation of the in-plane magnetic field. In the presence of a strong magnetic field, we observe a change of sign in the SDE. Simulation and measurement of supercurrent suggest that depending on the superconducting widths, W_S , this sign change may not necessarily be related to $0-\pi$ or topological transitions. We find that the strongest sign change in junctions with narrow W_S is consistent with SOC-induced asymmetry of the critical current under magnetic-field inversion, while in wider W_S , the sign reversal could be related to $0-\pi$ transitions and topological superconductivity.

Nonreciprocity in non-centrosymmetric quantum systems has been well studied in semiconductors as they are essential for the rectification function in electrical diodes and solar cells. There has been a recent rise of interest in nonreciprocity in superconductors, implying a progress toward designing superconducting diodes and its possible application in modern electronic circuits, sensors, and detectors^{1–12}. Nonreciprocal critical currents in superconductors occur when the magnitude of the critical supercurrent, I_c , depends on the direction in which the current is swept. Theoretically, the so-called diode effect can occur when both inversion and time-reversal symmetries are broken, where the latter can be achieved by the magnetic proximity effect, in magnetic Josephson junctions, or by applying an external magnetic field. This effect has been attributed to the presence of finite-momentum Cooper pairs and the change in the nature of superconductivity^{7,13–16}. Recent studies have suggested the existence of the superconducting diode effect (SDE) in Josephson junctions (JJs) with large Rashba spin-orbit coupling (SOC)^{1,2,5,6,17–19}. The magnitude of the supercurrent in JJs with SOC depends on the direction of the magnetic field, as the Rashba and Dresselhaus effects can have different contributions^{20,21}. Therefore, investigating the SDE through a JJ can provide information about the SOC in its semiconductor.

Planar JJs fabricated on epitaxial Al-InAs heterostructures are great candidates to study SDE due to their strong SOC^{2,3,22}. Such devices have also shown signatures of topological phase transition when their time-reversal symmetry is broken by an in-plane magnetic field^{13–25}. Recently, Costa et al.¹⁷

have reported a sign reversal of the AC SDE in multi-channel JJs based on Al-InAs with strong SOC subjected to a magnetic field, and related it to a $0-\pi$ -like transition induced by the Zeeman interaction in the device. Conversely, Banerjee et al.²⁵ have proposed a SDE originating from finite-momentum Cooper pairing solely due to orbital effects, without invoking SOC or Zeeman interaction.

In this work, we study epitaxial Al-InAs JJs with various superconductive contact widths, W_S . By applying a magnetic field perpendicular to the current and parallel to the junction, we observe nonreciprocal critical currents due to the finite-momentum Cooper pairing enabled by the coexistence of strong Rashba SOC and the Zeeman interaction. We observe a SOC-induced shift, B_* , of the magnetic field yielding the maximum of the critical current amplitude and use it to estimate the Rashba SOC strength in the JJ. In the absence of the magnetic field, time-reversal symmetry is restored and the SDE vanishes. However, the SDE can also vanish at certain finite magnetic fields and changes sign below the superconductor critical field, B_c . We consider JJs with various superconducting widths, W_S , and observe zeros of the SDE, across which the critical current difference $\Delta I_c = I_c^+ - |I_c^-|$ characterizing the SDE exhibits sign reversals at finite values of the magnetic field. We attribute the sign reversals to (i) $0-\pi$ -like jumps of the ground-state superconducting phase difference for wide W_S and (ii) SOC-induced asymmetry of the critical current under magnetic field inversion with respect to the field shift, B_* for narrow W_S . In a gated junction, we observe the

¹Center for Quantum Information Physics, Department of Physics, New York University, New York, NY, USA. ²Department of Physics & Astronomy, Wayne State University, Detroit, MI, USA. ³Department of Physics, University at Buffalo, State University of New York, Buffalo, NY, USA. ✉e-mail: jshabani@nyu.edu

SDE and SOC-induced shift at zero and positive gate voltages where the SOC is strong in our system. However, the SDE is negligible when a negative gate voltage is applied, suggesting that the Rashba strength is relatively small at negative gate voltages. This agrees with our previous studies of SOC strength measurements on gated Hall bars.

Results and discussion

Devices and measurement details

Our junctions are based on epitaxial superconducting Al thin films grown in situ on InAs heterostructures by molecular beam epitaxy on a InP substrate followed by a graded buffer layer^{22,26,27}. Typically, the critical field of thin film of Al is greater than 1 T. Figure 1a shows a general schematic of our planar JJs. We study junctions with varying superconducting widths from $W_S = 0.15 \mu\text{m}$ to $W_S = 1 \mu\text{m}$. All the junctions are $W = 4 \mu\text{m}$ wide and are fabricated using Transene selective wet etching of Al. Figure 1b shows a false-colored scanning electron microscopy (SEM) image of a typical $L = 150 \text{ nm}$ long junction with superconducting width of $W_S = 1 \mu\text{m}$. The Al-induced gap in our junctions is about $\Delta = 220 \mu\text{eV}$ estimated from

critical temperature, T_c . The semiconductor-superconductor transparency of our junctions are reported in our previous works²⁸⁻³⁰ and can host modes with near unity transparency. All the measurements in this study are performed at $T \approx 30 \text{ mK}$ in a dilution refrigerator equipped with a three-axis vector magnet. As shown in Fig. 1b, the z axis of the magnet is perpendicular to the sample plane, while x and y axes are in-plane components aligned parallel to the current and junction, respectively.

Figure 1c presents the differential resistance as a function of the bias current and applied out-of-plane magnetic field for the junction JJ1 with $W_S = 0.6 \mu\text{m}$ when the in-plane field is set to zero. The observed Fraunhofer pattern shows a hysteresis due to heating effects when bias is swept through zero^{28,31}. The critical current of the hot electrons branch, where the bias goes from high bias to zero, is clearly smaller than the critical current of the cold electrons branch going from zero to high bias. This is due to the difference between the effective electronic temperature of the hot and cold electrons branches before the transition to or out of the superconducting state. Such a hysteretic behavior leads to different values of critical current on each side, as can be observed in Fig. 1d for JJ1, and has to be avoided for accurate SDE

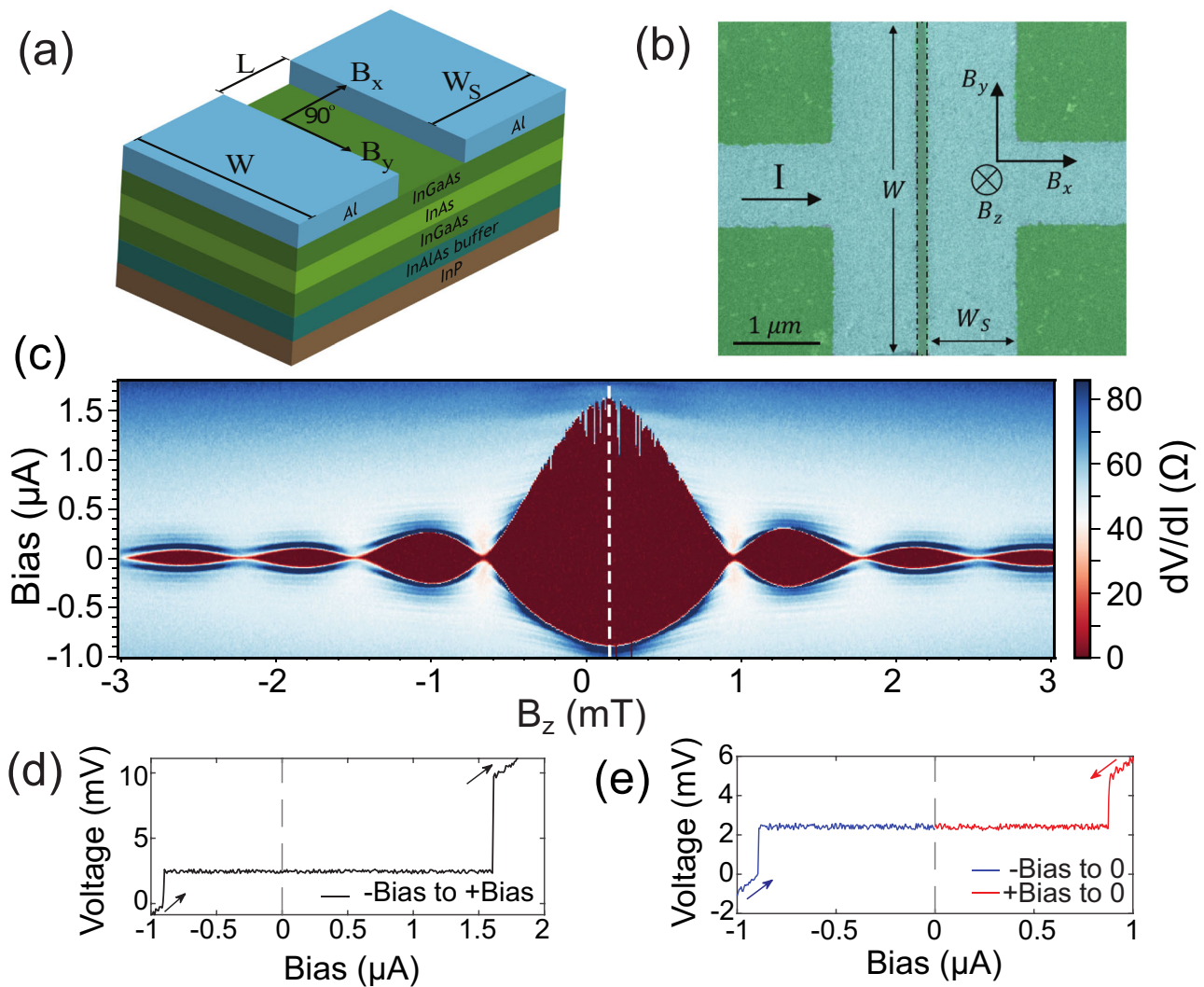


Fig. 1 | Devices and measurement methods. **a** A schematic of a junction of length L , width W and superconducting width of W_S fabricated on the Al-InAs heterostructure. The superconducting contacts are made of Al and the quantum well (QW) consists of a layer of InAs grown between two layers of $\text{In}_{0.81}\text{Ga}_{0.19}\text{As}$. **b** False-colored SEM image of a typical junction showing Al (blue) and QW (green) regions. The dashed line between the superconducting contacts is the $W = 4 \mu\text{m}$ wide and $L = 150\text{-nm}$ -long etched gap. The magnetic field can be applied in three direction independently as shown on the SEM image. **c** Differential resistance as a function of

the bias current and out-of-plane magnetic field of Josephson junction 1 (JJ1) with $W_S = 0.6 \mu\text{m}$ at zero in-plane magnetic field. A hysteresis due to the thermal effects can be seen. White dashed line indicates the position of the maximum of the critical current. **d** A line cut of (c) showing hysteresis in voltage versus current when the bias is swept from negative to positive. The values of supercurrent on each side are different due to the thermal effects. **e** Voltage versus current when the bias is swept from negative to zero (blue) and positive to zero (red). The values of supercurrent on two sides are expected to be equal in a conventional JJ.

measurements. In addition, Fig. 1c shows that the cold electron branch exhibits a broad switching distribution near the Fraunhofer maximum with several premature switching events. For the rest of this study, we therefore only derive the values of the critical current from the hot electrons branch, going from high bias to zero bias as shown in Fig. 1e. These two values, i.e., the positive and negative retrapping currents, are expected to be equal in magnitude in reciprocal measurements of a conventional device without the presence of in-plane magnetic field.

Low in-plane field dependence

By carefully aligning the magnet directions to the Josephson junction and eliminating unwanted out-of-plane component of magnetic field (B_z), we measure the critical current in the presence of an in-plane magnetic field. Figure 2a, b shows the measured magnitude of the critical current $|I_c|$ for JJ1 with $W_S = 0.6 \mu\text{m}$ and JJ2 with $W_S = 0.15 \mu\text{m}$ when $B_z = 0 \text{ T}$ and the in-plane magnetic field with strength B_x is parallel to the current. Blue circles and red cross marks correspond to the measurement of the magnitude of the critical current when the bias is swept from negative high bias to zero and from positive high bias to zero, respectively. We find that the magnitude of the critical current in both directions is the same and there is no sign of nonreciprocity when the applied in-plane magnetic field is parallel to the current. The absence of SDE when the field is parallel to the current indicates that the dominant SOC in the junctions is of Rashba type, which is in agreement with our previous works^{26,32}.

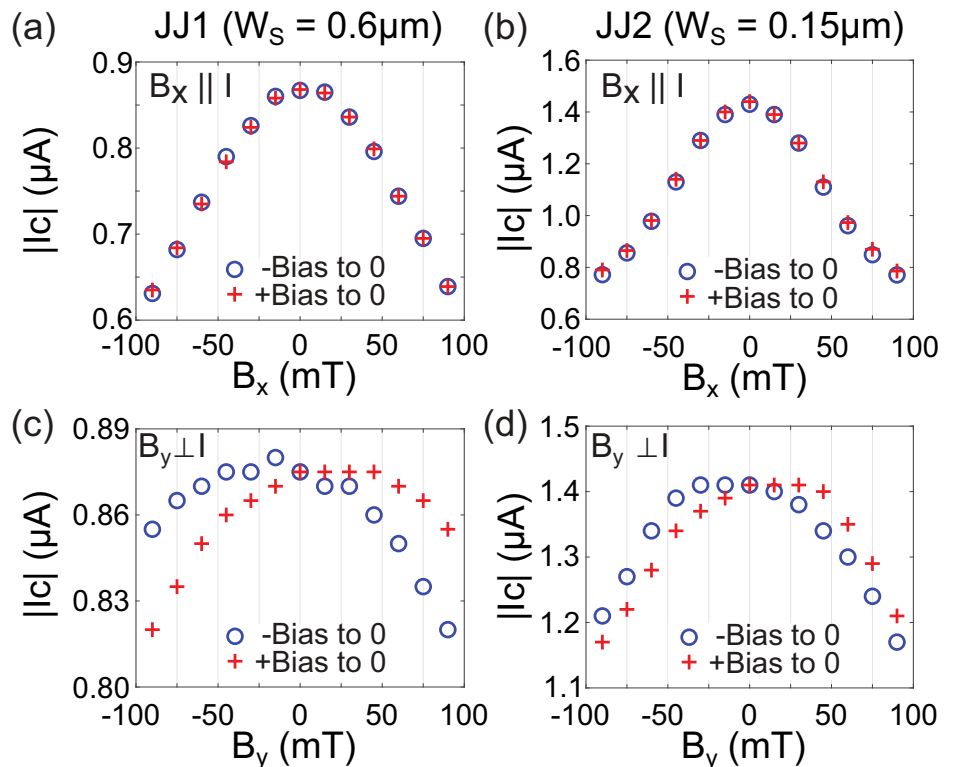
When the in-plane magnetic field is applied perpendicular to the current, in the y -direction, we find a difference between the forward and reverse critical currents. Figure 2c, d shows the dependence of the absolute value of critical current $|I_c|$ on B_y for JJ1 and JJ2. We observe a clear non-reciprocal behavior, where the critical current is larger for positive than for negative bias when $B_y > 0$. This behavior is reversed when the in-plane field direction is flipped to $B_y < 0$, in agreement with the theoretically expected symmetry relation $I_c^+(B_y) = |I_c^-(-B_y)|$. Details of the experimental measurements and analyses are given in Supplementary Note 1. We extract I_c at each in-plane magnetic field from the maximum of the Fraunhofer pattern at that field (see Supplementary Figs. S3 and S4 for more details). The same

measurements were done on three additional devices with $W_S = 0.4, 0.8,$ and $1 \mu\text{m}$ and showed the same results, as presented in Supplementary Figs. S5 and S6 of Supplementary Note 1. Those devices exhibit the same behavior as JJ1 and JJ2. In all cases, we observe a shift, B_* in the magnetic fields at which the critical currents reach their maximum values when $B_y \perp I$. The shift is positive for the critical current corresponding to positive bias and negative for the case of negative bias. In JJ1 and JJ2, the magnitude of shift on both negative and positive sides are the same and equal to $|B_*| = 15 \text{ mT}$. Although the value of $|I_c|$ at few magnetic fields are very close to each other, but from the zoom-in plots of the data presented in Supplementary Figs. S7–S9 for JJ1, we can see that the maximum of $|I_c|$ is at 15 mT for both positive and negative fields (dashed black line in both figures).

This observed shift is captured by our numerical tight-binding simulations (see details in Supplementary Note 2). The result of the tight-binding simulation in Supplementary Fig. S13a for a junction with $W_S = 0.15 \mu\text{m}$ clearly shows the superconducting diode effect in the splitting of I_c^\pm , as well as the symmetry with respect to the sign of B_y . Moreover, B_* indicates the presence of SOC in the junction and obeys the symmetry relation, $B_*(\alpha) = -B_*(-\alpha)$, where α denotes the strength of the Rashba SOC. (We neglect Dresselhaus SOC for simplicity, as Rashba SOC is typically dominant in this system³²). As an illustration, we perform numerical calculations of the magnetic field dependence of the critical currents for JJ2 and different values of the Rashba SOC strength. By tracking the fields at which the numerically calculated critical current maxima occur, we extract the α -dependence of B_* (see Supplementary Fig. S13b). The black, dashed line is just a linear fit to guide the eye. Comparing the field-shift value extracted from the experimental and the corresponding numerical simulations, we estimate the Rashba SOC strength in device JJ2 to be about 10 meV nm . This value is in overall agreement with values of α in InAs extracted through weak antilocalization measurements^{26,32}. Although Supplementary Fig. S13b was specifically computed for JJ2, from the fabrication process and similar composition, we expect all the samples to have similar SOC strengths.

Complementary to the numerical simulations, we provide approximate analytical expressions for the normalized critical currents at low field

Fig. 2 | Low in-plane magnetic field dependence. Absolute value of the critical currents as a function of the in-plane magnetic field for (a, c) Josephson junction 1 (JJ1) and (b, d) JJ2, with superconducting contact widths W_S indicated. a, b and c, d correspond to an in-plane magnetic field parallel and perpendicular to the current, respectively. The blue circles represent the magnitude of supercurrent when the bias is swept from negative to zero while red cross marks are for bias from positive to zero. The critical current amplitudes when the magnetic field is parallel to the current ($B \parallel \hat{x}$) are nearly equal in both directions, indicating a vanishing superconducting diode effect (SDE) (a, b). When the magnetic field is perpendicular to the current ($B \parallel \hat{y}$), the amplitudes of the forward and reverse critical currents are different, signaling the presence of the SDE (c, d). Note that nonreciprocity can be observed in both devices.



(see Supplementary Note 2 for detailed information),

$$\frac{|I_c^\pm|}{I_0} = 1 - b \left[1 \pm c \operatorname{sgn}(B_y \mp B_*) \right] (B_y \mp B_*)^2, \quad (1)$$

where I_0 is the maximum absolute value of the critical current, $b = (g^* \mu_B / 4E_T)^2$, $c = k_{so} / k_F$, and $B_* \approx (1 - \tau)^{1/4} (c / \sqrt{b})$ (with τ as the junction transparency) is the magnitude of the field at which I_c is maximum. Here g^* is the effective g-factor, μ_B the Bohr magneton, k_F the Fermi wave vector, $E_T = \hbar v_F / (2L)$ the Thouless energy, v_F the Fermi velocity, and $k_{so} = \alpha m^* / \hbar^2$, with m^* representing the effective mass. As discussed in Supplementary Note 2, Eq. (1) was obtained in the limits $L \ll \xi_0$ where ξ_0 is the superconducting coherence length and $W_S \rightarrow \infty$, assuming the Zeeman interaction is sizable in the N region only, and again neglecting Dresselhaus SOC. Therefore it is not in quantitative agreement with finite W_S in experimental devices. However, Eq. (1) can provide a qualitative description of the main trends exhibited by the critical currents. In fact, Eq. (1) reproduces well the functional behavior of the experimental data at low field. Supplementary Fig. S10 shows the experimental data of all the junctions studied fitted to Eq. (1) using b , c and B_* as fitting parameters, while Supplementary Fig. S11 shows that W_S is not predictive of the B_* observed in the presented devices. According to the simplified analytical model, the asymptotic behavior of B_* at low magnetic fields does not only depend on the SOC strength but also on other system parameters, like the junction transparency (see Supplementary Note 2 and ref. 33). Hence devices exhibiting larger values of B_* (see bottom row of Supplementary Fig. S10) may still have similar SOC strength with lower transparency.

Our experimental data together with numerical simulation suggest that the observed SDE originates from the finite-momentum Cooper pairing induced by the shift of the Fermi contours when the Zeeman interaction and the Rashba SOC coexist as illustrated in Supplementary Fig. S13c–e. This picture implicitly follows from the microscopic model used in the numerical simulations, which in turn are able to explain the trends observed in the experimental data. Note that the observed SDE depends on both the magnetic field strength and direction. Therefore, the non-intrinsic contributions to the SDE originating from gate-dependent effective disorder in the superconducting electrodes³⁴, which are independent of the magnetic field, can be ruled out in our devices. Vortex asymmetric motion, another mechanism that may induce a nonreciprocal behavior^{35–37}, can also be disregarded as the origin of the SDE in our samples. Indeed, vortex asymmetric motion is expected to be relevant near the superconducting transition when the temperature and/or the applied field are close to their superconducting critical values. However, the SDE here reported is finite at magnetic fields as low as few mT (i.e., at fields much smaller than the critical field $B_c \approx 1.6$ T) and temperature of 30 mK (well below $T_c \approx 1.5$ K).

In the regime $E_Z \ll \alpha k_F$, where E_Z , α , and k_F denote the Zeeman energy, the Rashba SOC strength and the Fermi wave vector, respectively, the Fermi contours in the N region can be approximated as,

$$k_\lambda = -\lambda k_{so} + \sqrt{k_F^2 + k_{so}^2 + \lambda \kappa^2 \sin(\varphi - \theta)}, \quad (2)$$

where $\lambda = \pm 1$, $\kappa = \sqrt{2m^* E_Z / \hbar^2}$, and θ and φ determine the directions of the wave vector and magnetic field with respect to the x axis, respectively. The x -component of the total momentum of the pairs is,

$$q \approx \frac{\kappa^2 \sin \varphi}{\sqrt{k_F^2 + k_{so}^2}} \quad (3)$$

and the Cooper pair wave function across the junction can be approximated as,

$$|\psi\rangle = |\uparrow\downarrow\rangle e^{iqx} + |\downarrow\uparrow\rangle e^{-iqx} \quad (4)$$

and can be rewritten in terms of singlet, $|S\rangle = |\uparrow\downarrow\rangle + |\downarrow\uparrow\rangle$ and triplet, $|T\rangle = |\uparrow\downarrow\rangle - |\downarrow\uparrow\rangle$ components³⁸,

$$|\psi\rangle = \cos(qx)|S\rangle + i \sin(qx)|T\rangle. \quad (5)$$

For $E_Z \ll \alpha k_F$, an inversion of the magnetic field orientation reverses the direction of the Fermi contours shift without affecting the spin orientation. Therefore, the coexistence of the singlet and triplet components in the presence of SOC breaks the inversion symmetry of the wave function with respect to the magnetic field direction, resulting in a nonreciprocal response with distinct forward and reverse critical currents. However, the SDE vanishes when the magnetic field is oriented along the x axis (see Fig. 2a, b) for in this case $\varphi = 0$ and $q = 0$ in Eq. (3).

High in-plane field dependence

We further investigate the nonreciprocity of the critical currents at higher in-plane magnetic fields perpendicular to the current (B_y) in the devices JJ1 and JJ2. Figure 3a, b shows the absolute value of the critical currents for each junction as a function of B_y . A dip and peak in $|I_c|$ of JJ1 is observed around $B_y \sim 0.6$ T. Previous studies have suggested such a behavior can be related to the closing and reopening of the superconducting gap^{24,39} and a topological phase transition. Our numerical simulations exhibit a phase transition at magnetic field near 0.6 T for $W_S = 0.6 \mu\text{m}$ as shown in Supplementary Fig. S14. In contrast, JJ2 data do not show any peak or dip in the supercurrent in Fig. 3b. Numerical simulations also do not show a phase transition for the ground state of JJ2 with $W_S = 0.15 \mu\text{m}$ below 1 T as shown in Supplementary Fig. S15.

Figure 3c plots the difference between the absolute values of the critical currents for positive and negative biases $\Delta I_c = I_c^+ - |I_c^-|$, as a function of B_y . The results evidence the anti-symmetric character of ΔI_c , which for both junctions changes its sign when the magnetic field B_y is inverted. However, ΔI_c also exhibit zeros at certain values of B_y , across which sign reversals not related to magnetic field inversion are observed. This is particularly apparent for the device JJ2 (blue symbols) at fields $B_y \approx \pm 0.35$ T, as shown in Fig. 3c.

From a comparison between the experimental results and the numerical simulations, we identify two possible mechanisms responsible for the zeros of ΔI_c and their associated SDE sign reversals. According to Eq. (1), the SOC induces an asymmetry in the critical currents under the magnetic field inversion with respect to B_* , with $|I_c^\pm(B_* + \delta B)| \neq |I_c^\pm(B_* - \delta B)|$. This asymmetry is apparent in Figs. 2c, d and 3a, b. The coexistence of a finite magnetic shift, B_* , and a strong SOC-induced critical current asymmetry can cause $|I_c^+|$ and $|I_c^-|$ to cross at a finite magnetic field and produce a sign reversal in the SDE without involving $0-\pi$ -like transitions. This situation is apparent in JJ2 from Fig. 3b, c, where a critical current crossing and corresponding sign reversal of ΔI_c at $B_y \approx 0.35$ T are observed, respectively. The numerical simulations are in good agreement with the experimental data of JJ2, predicting a critical current crossing at $B_y = 0.4$ T, which is unrelated to the $0-\pi$ transition at $B_y \approx 1$ T (see Fig. S15 in Supplementary Note 2).

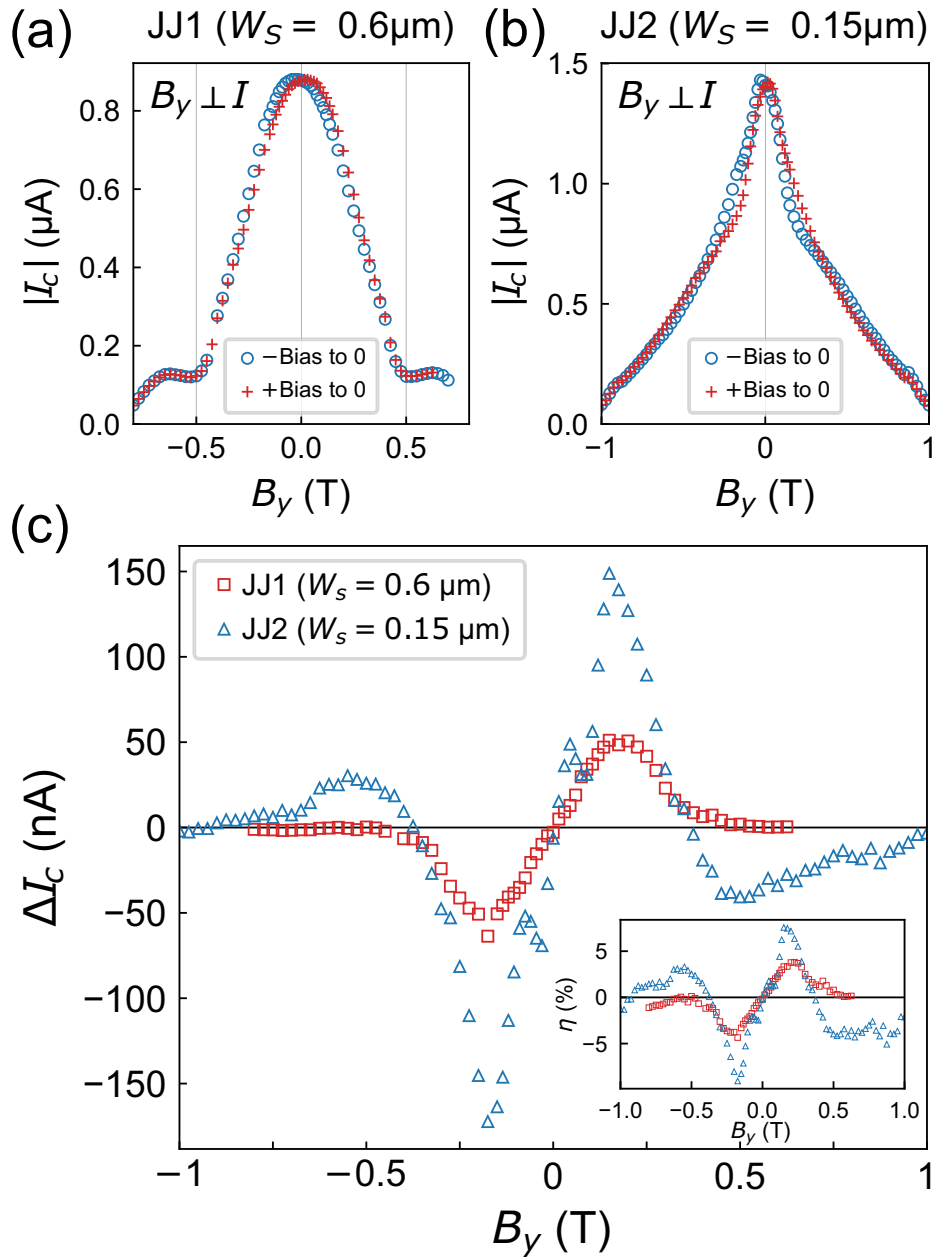
As discussed above, the SDE originates from finite-momentum Cooper pairing qualitatively described by a wave function lacking inversion symmetry with respect to B_y when both Rashba SOC and Zeeman interaction are present. However, it follows from Eq. (5) that the inversion symmetry with respect to B_y is reestablished when either the singlet or triplet component vanishes at the S/N interfaces located at $x = 0$ and $x = L$, i.e., when $|q|L = n\pi/2$, where n is an integer number. Therefore, junctions with $L \ll \xi_0 \ll W_S$ exhibit zeros of ΔI_c when,

$$B_y \approx n \frac{\pi}{g^* \mu_B} E_T \left(1 + \frac{k_{so}^2}{2k_F^2} \right) r_l. \quad (6)$$

The re-scaling factor $r_l = L / (2W_S + L)$ has been introduced to account for the fact that the Zeeman field is likely present over the whole system and not only in the semiconductor region.

The zeros (and their associated SDE sign reversals) corresponding to odd integers in Eq. (6), say $n = (2m + 1)$ (with m an integer), can be

Fig. 3 | High in-plane magnetic field dependence and sign change. Absolute value of supercurrent as a function of in-plane magnetic field perpendicular to the current in (a) Josephson junction 1 (JJ1), and (b) JJ2 at high magnetic fields, with superconducting contact widths W_S indicated. The blue circles represent the magnitude of supercurrent when the bias is swept from negative to zero while red cross marks are for bias from positive to zero. c Difference $\Delta I_c = I_c^+ - |I_c^-|$ between the absolute value of the critical currents measured under positive and negative biases as a function of B_y . Red squares and blue triangles correspond to JJ1, and JJ2, respectively. Inset: diode efficiency $\eta = (I_c^+ - |I_c^-|)/(I_c^+ + |I_c^-|)$.



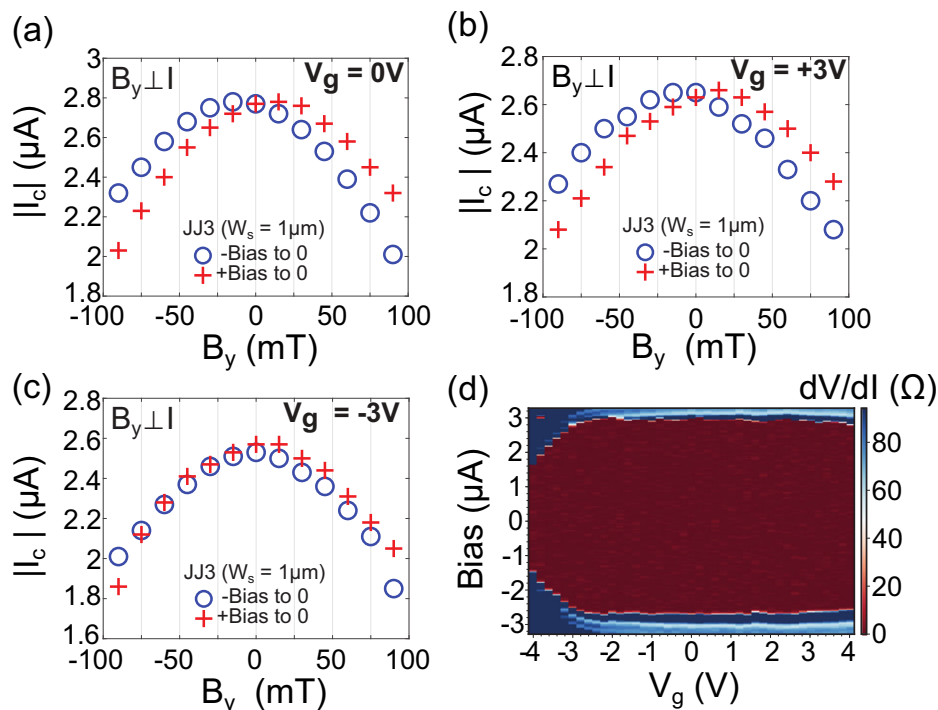
associated with $0-\pi$ -like transitions the junction would experience close to equilibrium. Indeed, in the absence of currents, the superconducting phase difference self-tunes to a value ϕ_{GS} (referred to as the ground-state phase difference) that minimizes the free energy of the system. For $\cos(qL) > 0$ the singlet component of the wave function at the two superconducting leads has the same sign, indicating that $\phi_{GS} = 0$. However, when $\cos(qW_L) = 0$ (i.e., $qL = (2m + 1)\pi/2$), the ground-state phase jumps from 0 to π and the singlet at the two superconducting leads acquire opposite signs for $\cos(qL) > 0$. Therefore, SDE sign reversals corresponding to odd values of n in Eq. (6) are associated to $0-\pi$ -like (or $\pi-0$ -like) transitions, while additional sign reversals are expected to occur between $0-\pi$ and $\pi-0$ -like transitions, when n is even. The $0-\pi$ -like ground-state phase jump has been identified as a possible signature of topological phase transitions in planar JJs^{24,39}. Hence, the nodes of ΔI_c corresponding to odd n may indirectly signal a transition into the topological superconducting state. However, such a signature is not conclusive, especially in JJs with narrow superconducting leads, where ground-state phase jumps are not necessarily associated to topological phase transitions^{40,41}.

The numerical simulations for devices JJ1 and JJ2 reveal $0-\pi$ -like jumps of the ground-state phase at $B_y \approx \pm 0.6$ T and $B_y \approx \pm 1$ T, respectively (see Supplementary Figs. S13 and S14b in Supplementary Note 2), suggesting that if the ΔI_c changes sign at higher fields (see insets in Fig. 3c) they could be associated to $0-\pi$ -like transitions with $n = 1$. However, we find that the measured current difference, ΔI_c , is too small in experiment and is difficult to conclusively establish the existence of these sign reversals in range of 0.6 T to 1 T.

Gate dependence

To further investigate the effect of SOC on the SDE, we make a gated device JJ3 with $W_S = 1.0 \mu\text{m}$ by depositing 60 nm Al_2O_3 followed by 5/40 nm Cr/Au on the junction. The thickness of Al in JJ3 is 8 nm and the QW has the exact same structure as the QW in other junctions in this study. Figure 4a-c shows the measured magnitude of the critical current of JJ3 at three different gate voltages when $B_z = 0$ and the in-plane magnetic field is perpendicular to the current (B_y). A clear nonreciprocal behavior can be seen when $V_g = 0$ and +3 V. However, the SDE is negligible when $V_g = -3$ V. It has been

Fig. 4 | Gate dependence at low in-plane magnetic field. Absolute value of the critical currents I_c as a function of the in-plane magnetic field perpendicular to the current $B \parallel \hat{y}$ for the gated Josephson junction (JJ3) with superconducting contact width $W_s = 1.0 \mu\text{m}$ at three different gate voltages: **a** $V_g = 0 \text{ V}$, **b** $V_g = 3 \text{ V}$, and **c** $V_g = -3 \text{ V}$. The blue circles represent the magnitude of supercurrent when the bias is swept from negative to zero while red cross marks are for bias from positive to zero. The nonreciprocity can be observed when the gate voltage is $V_g = 0, +3 \text{ V}$, indicating the presence of the superconducting diode effect (SDE) (**a**, **b**). When the gate voltage is $V_g = -3 \text{ V}$, the amplitudes of the forward and reverse critical currents are almost the same, indicating a vanishing of the SDE (**c**). **d** Differential resistance of JJ3 as a function of the bias current and applied gate voltage at zero field. Here, the bias was swept from negative to positive values: the difference in positive and negative critical current observed is a hysteretic artifact, see Fig. 1c, d and the surrounding discussion.



reported that in InSb nanowires, the SDE drastically depends on the applied gate and orientation of magnetic field and can be suppressed in the absence of SOC in the system⁸. In previous studies of SOC effects in our system with gated Hall bar measurements, we reported that the Rashba strength can be tuned by gate voltage and is smaller at low densities^{26,32}. Figure 4d shows the differential resistance of JJ3 as a function of bias and gate voltage at zero magnetic field. At $V_g = -3 \text{ V}$ the density is much lower than $V_g = 0$ and $+3 \text{ V}$. The absence of SDE in Fig. 4c suggests that at $V_g = -3 \text{ V}$ the Rashba parameter is significantly smaller than the SOC strength at zero and positive gate voltages.

Conclusion

In summary, we have studied the superconducting diode effect in epitaxial InAs/Al Josephson junctions with different superconducting width and showed that the SDE depends on the orientation of the applied in-plane magnetic field in the system. By measuring the supercurrent of the junction, we observe SDE only when the in-plane field is perpendicular to the current. We observe a shift in magnetic field yielding the maximum critical current and obtain an analytical expression describing the critical current behavior at low magnetic field. We propose a method for estimating the Rashba parameter from the measurement of the magnetic field shift of the SDE and numerical simulations. The results are in good agreement with values previously reported for our system. We also measure the SDE at high magnetic fields and observe a sign change in the ΔI_c of the $W_s = 0.15 \mu\text{m}$ junction at $B_y \approx \pm 0.35 \text{ T}$. Using our Tight-binding simulation, we conclude that this sign change is not necessarily an indicator of $0-\pi$ or topological transitions in the system. By measuring the SDE in a gated junction at three different gate voltages, we showed that the SDE strongly depends on the applied gate voltage and the SOC strength in our system.

Methods

Wafers are grown by molecular beam epitaxy. Devices are fabricated using a combination of wet etching and deposition techniques after patterning polymethyl methacrylate (PMMA) via electron beam lithography. Device mesa features are defined by a deep wet etch with 85% concentrated phosphoric acid, 30% concentrated hydrogen peroxide, and deionized water in a volumetric ratio of 1:1:40 after selectively etching the aluminum top

layer with Transene Aluminum Etchant Type D. Junction weak links and smaller device features are defined by a subsequent aluminum etch. Gated devices subsequently undergo dielectric deposition of aluminum oxide via atomic layer deposition, and titanium/gold gates are deposited via electron beam evaporation. D.c. measurements are performed in a dilution refrigerator at a temperature of around 30 mK using standard low-frequency lock-in amplification techniques with excitation currents of at most 10 nA and frequencies of around 17 Hz. Magnetic field is generated by a three-axis superconducting vector magnet.

Data availability

The transport data generated in relation to this study are available in Zenodo (<https://doi.org/10.5281/zenodo.10810819>)⁴².

Code availability

All code related to this work is available from the corresponding author upon request.

Received: 24 October 2023; Accepted: 2 April 2024;

Published online: 06 April 2024

References

- Ando, F. et al. Observation of superconducting diode effect. *Nature* **584**, 373–376 (2020).
- Baumgartner, C. et al. Effect of Rashba and Dresselhaus spin-orbit coupling on supercurrent rectification and magnetochiral anisotropy of ballistic Josephson junctions. *J. Phys. Condens. Matter* **34**, 154005 (2022).
- Baumgartner, C. et al. Supercurrent rectification and magnetochiral effects in symmetric Josephson junctions. *Nat. Nanotechnol.* **17**, 39–44 (2022).
- Bauriedl, L. et al. Supercurrent diode effect and magnetochiral anisotropy in few-layer NbSe_2 . *Nat. Commun.* **13**, 4266 (2022).
- Wu, H. et al. The field-free Josephson diode in a van der Waals heterostructure. *Nature* **604**, 653–656 (2022).
- Pal, B. et al. Josephson diode effect from Cooper pair momentum in a topological semimetal. *Nat. Phys.* **18**, 1228–1233 (2022).

7. Yuan, N. F. Q. & Fu, L. Supercurrent diode effect and finite-momentum superconductors. *Proc. Natl. Acad. Sci. USA* **119**, e2119548119 (2022).
8. Mazur, G. P. et al. The gate-tunable Josephson diode. Preprint at <https://arxiv.org/abs/2211.14283> (2022)
9. Sundaresh, A., Väyrynen, J. I., Lyanda-Geller, Y. & Rokhinson, L. P. Diamagnetic mechanism of critical current non-reciprocity in multilayered superconductors. *Nat. Commun.* **14**, 1628 (2023).
10. Gupta, M. et al. Gate-tunable superconducting diode effect in a three-terminal Josephson device. *Nat. Commun.* **14**, 3078 (2023).
11. Zhang, B. et al. Evidence of ϕ_0 -Josephson junction from skewed diffraction patterns in Sn-InSb nanowires. Preprint at <https://arxiv.org/abs/2212.00199> (2022).
12. Margineda, D. et al. Sign reversal diode effect in superconducting Dayem nanobridges. *Commun. Phys.* **6**, 1–9 (2023).
13. Davydova, M., Prembabu, S. & Fu, L. Universal Josephson diode effect. *Sci. Adv.* **8**, eabo0309 (2022).
14. Daido, A., Ikeda, Y. & Yanase, Y. Intrinsic superconducting diode effect. *Phys. Rev. Lett.* **128**, 037001 (2022).
15. Ilic, S. & Bergeret, F. Theory of the supercurrent diode effect in Rashba superconductors with arbitrary disorder. *Phys. Rev. Lett.* **128**, 177001 (2022).
16. He, J. J., Tanaka, Y. & Nagaosa, N. A phenomenological theory of superconductor diodes. *N. J. Phys.* **24**, 053014 (2022).
17. Costa, A. et al. Sign reversal of the Josephson inductance magnetochiral anisotropy and $0-\pi$ -like transitions in supercurrent diodes. *Nat. Nanotechnol.* **18**, 1266–1272 (2023).
18. Turini, B. et al. Josephson diode effect in high-mobility InSb nanoflags. *Nano Lett.* **22**, 8502–8508 (2022).
19. Jeon, K.-R. et al. Zero-field polarity-reversible Josephson supercurrent diodes enabled by a proximity-magnetized Pt barrier. *Nat. Mater.* **21**, 1008–1013 (2022).
20. Pakizer, J. D., Scharf, B. & Matos-Abiague, A. Crystalline anisotropic topological superconductivity in planar Josephson junctions. *Phys. Rev. Res.* **3**, 013198 (2021).
21. Pekerten, B., Pakizer, J. D., Hawin, B. & Matos-Abiague, A. Anisotropic topological superconductivity in Josephson junctions. *Phys. Rev. B* **105**, 054504 (2022).
22. Shabani, J. et al. Two-dimensional epitaxial superconductor-semiconductor heterostructures: a platform for topological superconducting networks. *Phys. Rev. B* **93**, 155402 (2016).
23. Fornieri, A. et al. Evidence of topological superconductivity in planar Josephson junctions. *Nature* **569**, 89–92 (2019).
24. Dartiailh, M. C. et al. Phase signature of topological transition in Josephson junctions. *Phys. Rev. Lett.* **126**, 036802 (2021).
25. Banerjee, A. et al. Phase asymmetry of Andreev spectra from cooper-pair momentum. *Phys. Rev. Lett.* **131**, 196301 (2023).
26. Wickramasinghe, K. S. et al. Transport properties of near surface InAs two-dimensional heterostructures. *Appl. Phys. Lett.* **113**, 262104 (2018).
27. Strickland, W. M., Hatefipour, M., Langone, D., Farzaneh, S. M. & Shabani, J. Controlling Fermi level pinning in near-surface InAs quantum wells. *Appl. Phys. Lett.* **121**, 092104 (2022).
28. Mayer, W. et al. Superconducting proximity effect in epitaxial al-InAs heterostructures. *Appl. Phys. Lett.* **114**, 103104 (2019).
29. Mayer, W. et al. Gate controlled anomalous phase shift in al/inas Josephson junctions. *Nat. Commun.* **11**, 212 (2020).
30. Dartiailh, M. C. et al. Missing Shapiro steps in topologically trivial Josephson junction on InAs quantum well. *Nat. Commun.* **12**, 78 (2021).
31. Courtois, H., Meschke, M., Peltonen, J. T. & Pekola, J. P. Origin of hysteresis in a proximity Josephson junction. *Phys. Rev. Lett.* **101**, 067002 (2008).
32. Farzaneh, S. M. et al. Observing magnetoanisotropic weak antilocalization in near-surface quantum wells. *Phys. Rev. Res.* **6**, 013039 (2024).
33. Costa, A., Fabian, J. & Kochan, D. Microscopic study of the Josephson supercurrent diode effect in Josephson junctions based on two-dimensional electron gas. *Phys. Rev. B* **108**, 054522 (2023).
34. Lo, S.-T. et al. Controllable disorder in a hybrid nanoelectronic system: realization of a superconducting diode. *Sci. Rep.* **3**, 2274 (2013).
35. Lustikova, J. et al. Vortex rectenna powered by environmental fluctuations. *Nat. Commun.* **9**, 4922 (2018).
36. Zhang, E. et al. Nonreciprocal superconducting NbSe₂ antenna. *Nat. Commun.* **11**, 5634 (2020).
37. Masuko, M. et al. Nonreciprocal charge transport in topological superconductor candidate Bi₂Te₃/PdTe₂ heterostructure. *NPJ Quantum Mater.* **7**, 104 (2022).
38. Eschrig, M. Spin-polarized supercurrents for spintronics: a review of current progress. *Rep. Prog. Phys.* **78**, 104501 (2015).
39. Pientka, F. et al. Topological superconductivity in a planar Josephson junction. *Phys. Rev. X* **7**, 021032 (2017).
40. Setiawan, F., Stern, A. & Berg, E. Topological superconductivity in planar Josephson junctions: narrowing down to the nanowire limit. *Phys. Rev. B* **99**, 220506(R) (2019).
41. Pakizer, J. D. & Matos-Abiague, A. Signatures of topological transitions in the spin susceptibility of Josephson junctions. *Phys. Rev. B* **104**, L100506 (2021).
42. Schiela, W. F. et al. Data from “superconducting diode effect sign change in epitaxial Al-InAs Josephson junctions”. <https://doi.org/10.5281/zenodo.10810819> (2024).

Acknowledgements

This work is supported in part by DARPA Topological Excitations in Electronics (TEE) program under grant No. DP18AP900007, the U.S. Office of Naval Research (ONR) through Grants No. N000142112450 and MURI No. N000142212764. B.P. and A.M.A. acknowledge support from ONR Grant No. N000141712793.

Author contributions

W.M.S. grew the material heterostructure. N.L. and P.Y. fabricated the devices. N.L., W.F.S. and B.H.E. performed the measurements. N.L. and W.F.S. performed the analysis. B.P. and A.M. performed the analytical calculations and numerical simulations. N.L., W.F.S., A.M. and B.P. wrote the manuscript. J.S. conceived the experiment.

Competing interests

The authors declare no competing interests.

Additional information

Supplementary information The online version contains supplementary material available at <https://doi.org/10.1038/s42005-024-01618-5>.

Correspondence and requests for materials should be addressed to Javad Shabani.

Peer review information *Communications Physics* thanks the anonymous reviewers for their contribution to the peer review of this work. A peer review file is available.

Reprints and permissions information is available at <http://www.nature.com/reprints>

Publisher's note Springer Nature remains neutral with regard to jurisdictional claims in published maps and institutional affiliations.

Open Access This article is licensed under a Creative Commons Attribution 4.0 International License, which permits use, sharing, adaptation, distribution and reproduction in any medium or format, as long as you give appropriate credit to the original author(s) and the source, provide a link to the Creative Commons licence, and indicate if changes were made. The images or other third party material in this article are included in the article's Creative Commons licence, unless indicated otherwise in a credit line to the material. If material is not included in the article's Creative Commons licence and your intended use is not permitted by statutory regulation or exceeds the permitted use, you will need to obtain permission directly from the copyright holder. To view a copy of this licence, visit <http://creativecommons.org/licenses/by/4.0/>.

© The Author(s) 2024